J Biomol NMR (2014) 59:15–22
DOI 10.1007/s10858-014-9820-8

COMMUNICATION

BSH-CP based 3D solid-state NMR experiments for protein resonance assignment

Chaowei Shi · Hannes K. Fasshuber · Veniamin Chevelkov · Shengqi Xiang · Birgit Habenstein · Suresh Kumar Vasa · Stefan Becker · Adam Lange

Received: 8 November 2013 / Accepted: 20 January 2014 / Published online: 1 March 2014

Abstract We have recently presented band-selective homonuclear cross-polarization (BSH-CP) as an efficient method for CO–CA transfer in deuterated as well as protonated solid proteins. Here we show how the BSH-CP CO–CA transfer block can be incorporated in a set of three-dimensional (3D) solid-state NMR (ssNMR) pulse schemes tailored for resonance assignment of proteins at high static magnetic fields and moderate magic-angle spinning rates. Due to the achieved excellent transfer efficiency of 33 % for BSH-CP, a complete set of 3D spectra needed for unambiguous resonance assignment could be rapidly recorded within 1 week for the model protein ubiquitin. Thus we expect that BSH-CP could replace the typically used CO–CA transfer schemes in well-established 3D ssNMR approaches for resonance assignment of solid biomolecules.

Keywords Solid-state NMR · Magic-angle spinning · BSH-CP · Protein resonance assignment · Ubiquitin

Electronic supplementary material The online version of this article (doi:10.1007/s10858-014-9820-8) contains supplementary material, which is available to authorized users.

C. Shi · H. K. Fasshuber · V. Chevelkov · S. Xiang · B. Habenstein · S. K. Vasa · S. Becker · A. Lange (✉)
Department of NMR-based Structural Biology, Max Planck Institute for Biophysical Chemistry, Am Fassberg 11, 37077 Göttingen, Germany
e-mail: adla@nmr.mpibpc.mpg.de

C. Shi
School of Life Sciences, University of Science and Technology of China, 96 JinZhai Road, 230026 Hefei, People's Republic of China

Introduction

Magic-angle spinning (MAS) solid-state NMR (ssNMR) has evolved in the past decade into a powerful technique to determine structure and dynamics of insoluble proteins (Goldbourt 2013; Knight et al. 2012; Sengupta et al. 2012) and protein complexes (Mainz et al. 2013), such as amyloid fibrils (Tycko 2011; Wasmer et al. 2008), membrane proteins (Hong et al. 2012; Ullrich et al. 2011) and oligomeric assemblies (Jehle et al. 2010; Loquet et al. 2012). This became possible in part due to the availability of higher external magnetic fields and the development of two-dimensional (2D) and three-dimensional (3D) homonuclear and heteronuclear correlation experiments.

The sequential resonance assignment is the basis of all further ssNMR spectroscopic studies (Pauli et al. 2001; Schuetz et al. 2010; Shi et al. 2009; Sperling et al. 2010). An important step was the development of efficient ^{15}N–^{13}C SPECIFIC-CP transfer which is widely used today (Baldus et al. 1998). Another crucial part in many protein sequential assignment schemes is the magnetization transfer between CO and CA nuclei. Here, a number of recoupling techniques have been employed so far, with the most widely used methods being proton-driven spin diffusion (PDSD) (Dusold and Sebald 2000), DARR/RAD (Morcombe et al. 2004; Takegoshi et al. 2001), MIRROR (Scholz et al. 2008) and DREAM (Verel et al. 2001). At stronger external magnetic fields, higher MAS frequencies are preferable for efficient CSA suppression to minimize spinning sidebands. Under these conditions (high field of 700–900 MHz, moderate MAS rate $\sim$20 kHz), PDSD, DARR and MIRROR become less efficient due to an increased Zeeman energy difference and better averaging of dipolar couplings. The DREAM scheme works well when the spinning rate considerably exceeds the isotropic

chemical shift difference of CO and CA spins (Laage et al. 2008; Vijayan et al. 2009), and thus it is more suitable for small rotor sizes with small active sample volume, which may not be favorable if enough sample is available to fill larger rotors (e.g. 3.2 mm outer diameter) (Demers et al. 2011).

Recently, robust and efficient band-selective homonuclear (BSH) cross-polarization between CO and CA spins was achieved by us in both highly deuterated (Chevelkov et al. 2013a) and protonated protein samples (Chevelkov et al. 2013b). The most efficient recoupling is achieved when the sum of effective radio-frequency fields on CO and CA resonances equals two times the spinning frequency, yielding up to 50 % of magnetization transfer efficiency in highly deuterated proteins and 33 % in protonated proteins. This compares very favorably to PDSD-type experiments which are often applied. Furthermore, different from the second-order PDSD/MIRROR phenomena, BSH-CP employs a first-order recoupling effect and undesired sequential or long-range magnetization transfers are suppressed (Chevelkov et al. 2013b; Hodgkinson and Emsley 1999).

Herein, we apply BSH-CP in a complete set of 3D protein sequential resonance assignment experiments, namely NCOCA, NCOCACB, and NCACO in addition to standard 3D NCACB and CANCO experiments. Using a set of the resulting five 3D spectra, reliable and unambiguous assignments can be obtained. Additionally, we discuss results from a 3D N(co)CACB spectrum which could be useful to assign larger proteins.

Results and discussion

Comparison of BSH-CP, MIRROR and DARR for CO–CA transfer

Previously, we compared in detail the performance of BSH-CP and PDSD CO–CA transfers in 1D and 2D experiments (Chevelkov et al. 2013b). Here, we compared the performance of BSH-CP with the performance of MIRROR and DARR in NCOCX experiments. Figure 1 shows 1D ^{13}C spectra obtained with BSH-CP NCOCA and NCOCX experiments based on MIRROR recoupling. The contact time of the BSH-CP step was 4.0 ms. The recoupling time for CO–CA transfer during MIRROR was 30 ms, which yields maximal CA signal. Panel b presents the dependence of CO–CA transfer on the employed ^{1}H CW recoupling RF field in the NCOCX experiment based on MIRROR and DARR recoupling. The maximum transfer rate was achieved with a proton field strength of 16 kHz, which corresponds to the MIRROR, $n = 2$ condition. The magnetization transfer efficiency at a proton RF

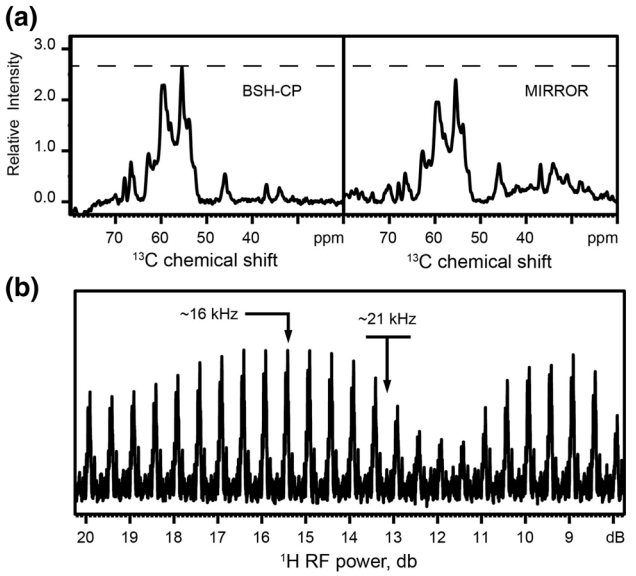

Fig. 1 **a** CA intensity after CO–CA transfer in BSH-CP based NCOCA and MIRROR based NCOCX experiments as indicated in the panels. The duration of the BSH-CP step was 4.0 ms, while the MIRROR contact time was 30 ms with a ^{1}H RF field strength set to 16 kHz. **b** CA signal after CO-CX magnetization transfer in a MIRROR/DARR based NCOCX experiment as a function of the applied ^{1}H RF field strength. The contact time was 20 ms. Experiments were recorded on a 850 MHz wide-bore spectrometer at an MAS rate of 21 kHz

field strength of 21 kHz, which corresponds to DARR, was extremely low at the given experimental conditions. The CA amplitude in the BSH-CP NCOCA experiment is ca. 1.12 times higher than in the MIRROR NCOCX experiment. Additionally, MIRROR is based on a second-order recoupling effect and facilitates long range magnetization transfers as well, which are not desirable in assignment experiments. In contrast, BSH-CP employs a first-order recoupling mechanism and unwanted sequential CO–CA and CA–CA transfers are efficiently suppressed by dipolar truncation.

Design of BSH-CP based 3D pulse schemes

The general pulse schemes for the collection of three-dimensional (3D) NCOCA, NCOCACB and NCACO spectra are presented in Fig. 2.

Initial ^{1}H–^{15}N magnetization transfer is achieved by cross polarization at the $n = 1$ Hartmann–Hahn condition. During the subsequent ^{15}N indirect evolution period, a hard 180° pulse is applied on the carbon channel to refocus ^{15}N–^{13}C scalar couplings. Next, a double quantum (DQ) SPECIFIC-CP step is used for the ^{15}N–^{13}C transfer (Baldus et al. 1998; Vijayan et al. 2009), followed by ^{13}C indirect evolution where another hard 180° pulse is applied on the nitrogen channel.

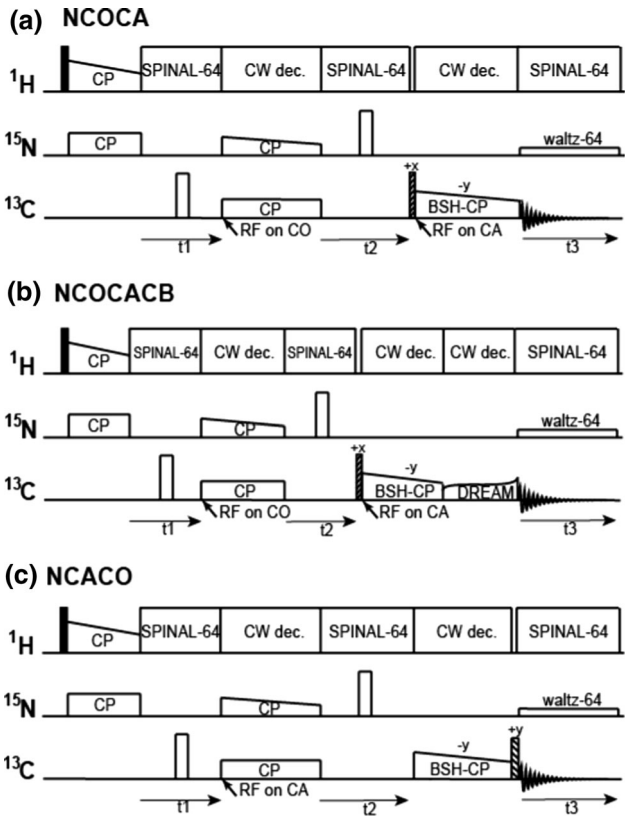

Fig. 2 The general pulse sequences for **a** 3D NCOCA, **b** 3D NCOCACB and **c** 3D NCACO correlation experiments based on band-selective homonuclear (BSH) CP transfer between CO and CA bands. *Open*, *filled* and *striped bars* represent hard 180°, 90° and trim pulses, respectively. The pulse scheme for the 3D N(co)CACB experiment which is a straightforward modification of the NCOCACB experiment can be found in Figure S1 (Supporting Information)

Homonuclear polarization transfer between CO and CA is achieved using the previously described BSH-CP transfer. Due to the fact that the chemical shift variation in the CO band is smaller than in the CA band, it is optimal to apply the RF irradiation in the middle of the CA region in order to avoid a too narrow banded transfer (see detailed explanation in ref. (Chevelkov et al. 2013a)). The theoretical RF field amplitude ω_{rf} is given by:

$$\sqrt{\Omega^2 + \omega_{rf}^2} + \omega_{rf} = 2\omega_r \quad (1)$$

where Ω is the CO chemical shift offset and ω_r the spinning frequency. For CO to CA magnetization transfer, the CO magnetization is flipped to the effective field by a hard trim pulse before BSH-CP (see Fig. 2 a, b). The flip angle θ is given by:

$$\theta = 90^\circ - \arctan\left(\omega_{rf}/\Omega\right) \quad (2)$$

For CA to CO magnetization transfer, a trim pulse is applied after BSH-CP, in order to bring the CO magnetization back to the transverse plane without affecting the CA magnetization (Fig. 2c).

In the 2D version of the NCOCA experiment (Chevelkov et al. 2013b) (dimension 1: N; dimension 2: CO, CA) it is important to maximize the CO signal by bringing it back to the transversal plane before detection by means of a second trim pulse after the BSH-CP part. In the 3D version (dimension 1: N; dimension 2: CO; dimension 3: CA) the CO signal is already recorded in the 2nd dimension. Applying a trim pulse will thus only affect the diagonal N–CO–CO peaks but not the real 3D N–CO–CA cross-peaks of interest.

Homonuclear polarization transfer from CA to CB in the NCOCACB experiment (see Fig. 2b), utilizes DREAM recoupling (Verel et al. 2001). SPINAL-64 decoupling (Fung et al. 2000) is applied on the proton channel during direct and indirect isotropic chemical shift evolution periods, and WALTZ-64 decoupling (Shaka et al. 1983) is applied on the nitrogen channel during detection to remove heteronuclear couplings. Continuous wave decoupling is applied on the proton channel during the SPECIFIC-CP, BSH-CP and DREAM transfer steps, respectively.

Application to MPD-crystallized ubiquitin and assignment strategy

As a first application of our 3D BSH-CP based experiments to resonance assignment, 3D NCOCA, NCOCACB, NCACO, and also standard 3D NCACB and CANCO spectra of MPD-crystallized uniformly [^{13}C,^{15}N]-labeled ubiquitin were recorded at 20 kHz MAS on an 800 MHz standard-bore spectrometer. Due to the combined effect of very efficient N–CO SPECIFIC-CP transfer at 20 kHz MAS (compared to low MAS rates ~11 kHz, see ref. (Chevelkov et al. 2013b)) and the high CO–CA transfer efficiency achieved using BSH-CP (33 %), the complete set of five 3D spectra could be recorded in 1 week with 3 s pre-scan delay (see Table 1) and the resulting spectra exhibit excellent sensitivity and resolution. A sequential walk along the backbone resonances can be easily obtained from a combination of all of these five spectra. A strip-plot showing the assignment procedure for a five-amino acid stretch is presented in Fig. 3.

Inter-residue spin system resonances (N_i, CA_{i-1}, CB_{i-1}, CO_{i-1}) could be determined from 3D NCOCA and NCOCACB spectra, while intra-residue spin system resonances (N_i, CA_i, CB_i, CO_i) were obtained from 3D NCACO and NCACB spectra. The assignment strategy is based on the principle that cross-peaks in the 3D CANCO spectrum correlate the resonance frequencies of three connected spins, two of which were identified in the previous step, and complemented by a new frequency of a further spin system. This strategy works in principle in both directions.

Table 1 Experimental parameters

Experiment	NCOCA	NCOCACB	N(co)CACB	NCACO	NCACB	CANCO
^{1}H Larmor freq. (MHz)	800	800	850	800	800	800
MAS rate (kHz)	20	20	21	20	20	20
Initial transfer	H–N, CP	H–N, CP	H–N, CP	H–N, CP	H–N, CP	H–C, CP
Field (kHz)-H	54.4	54.4	57.1	54.4	54.4	77.7
Field (kHz)-X	30.1	30.1	33.3	30.1	30.1	50.0
Shape	ramp100–80 H	ramp100–80 H	ramp100–80 H	ramp100–80 H	ramp100–80 H	ramp100–80 H
^{13}C carrier (ppm)	–	–	–	–	–	56.8
Time (ms)	0.34	0.34	0.34	0.34	0.34	0.19
Transfer 2	N–CO, SPECIFIC-CP	N–CO, SPECIFIC-CP	N–CO, SPECIFIC-CP	N–CA, SPECIFIC-CP	N–CA, SPECIFIC-CP	CA–N, SPECIFIC-CP
Field (kHz)-H	73.0	73.0	80.6	73.8	73.8	73.8
Field (kHz)-N	13.7	13.7	14.0	13.3	13.3	13.3
Field (kHz)-C	7.7	7.7	9.1	7.6	7.6	7.6
Shape	ramp100–80 N	ramp100–80 N	ramp100–80 N	ramp100–80 C	ramp100–80 C	ramp80–100 C
^{13}C carrier (ppm)	176.8	176.8	176.8	56.8	56.8	56.8
Time (ms)	4.1	4.1	4.1	3.9	3.9	3.9
Transfer 3	CO–CA, BSH-CP	CO–CA, BSH-CP	CO–CA, BSH-CP	CA-CO, BSH-CP	CA-CB, DREAM	N-CO, SPECIFIC-CP
Trim pulse	3.45 μs/50 kHz	3.45 μs/50 kHz	3.0 μs/55.5 kHz	–	–	–
Field (kHz)-H	75.5	75.5	80.6	75.5	73.8	73.0
Field (kHz)-N	–	–	–	–	–	13.7
Field (kHz)-C	14.2	14.2	13.8	14.6	11.1	7.7
Shape	ramp100–80 C	ramp100–80 C	ramp100–80 C	ramp100–80 C	ramp80–100 C	ramp100–80 N
^{13}C carrier (ppm)	56.8	56.8	57.2	56.8	56.8	176.8
Time (ms)	3.75	3.75	4.0	4.2	1.7	4.1
Trim pulse	–	–	–	5 μs/50 kHz	–	–
Transfer 4	–	CA-CB, DREAM	CA-CB, DREAM	–	–	–
Field (kHz)-H	–	73.8	80.6	–	–	–
Field (kHz)-C	–	11.1	10.6	–	–	–
Shape	–	ramp80–100 C	ramp80–100 C	–	–	–
^{13}C carrier (ppm)	–	56.8	40.0	–	–	–
Time (ms)	–	1.7	1.7	–	–	–
t1 evolution	N	N	N	N	N	CA
Field (kHz)-H	78.2	78.2	80.6	78.2	78.2	78.2
180^{o} pulse	C	C	C	C	C	N
Sweep width (kHz)	3.5	3.5	3.4	3.5	3.5	5.2
a.q. time (ms)	8.00	8.00	6.96	7.14	7.14	5.00
Increments	56	56	48	50	50	52
t2 evolution[a]	CO	CO	CA	CA	CA	N
Field (kHz)-H	78.2	78.2	80.6	78.2	78.2	78.2
180° pulse	N	N	N	N	N	C
Sweep width (kHz)	2.8	2.8	5.5	5.2	5.2	3.5
a.q. time (ms)	5.71	5.71	5.03	5.00	5.00	7.14
Increments	32	32	56	52	52	50
Detection (t3)	CO, CA	CO, CA, CB	CO, CA, CB	CO, CA	CA, CB	CO
Field (kHz)-H	78.2	78.2	80.6	78.2	78.2	78.2

Table 1 continued

Experiment	NCOCA	NCOCACB	N(co)CACB	NCACO	NCACB	CANCO
Sweep width (kHz)	59.5	59.5	64.1	59.5	59.5	59.5
a.q. time (ms)	8.94	7.98	7.94	8.94	8.94	8.94
Increments	1,064	950	1,018	1,064	1,064	1,064
Pre-scan delay (s)	3.0	3.0	3.0	3.0	3.0	3.0
Number of scans	16	32	16	16	16	8
Measurement time (h)	24.2	48.4	36.3	35.0	35.0	17.5

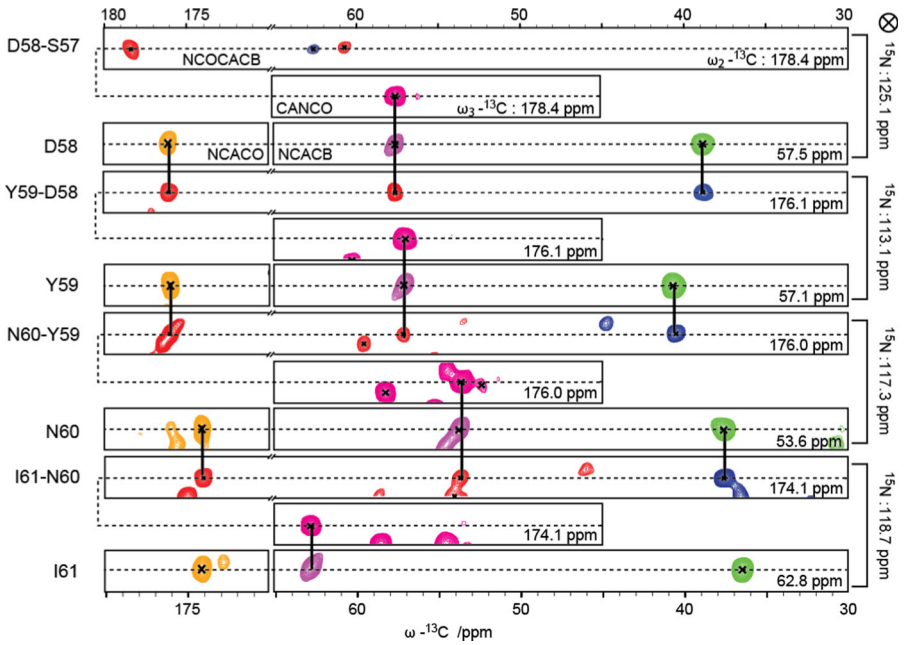

Fig. 3 Strip plot of different 3D experiments showing the sequential walk for the amino acid stretch D58-I61. NCOCACB spectra are presented in *red* (positive signals) and *blue* (negative signals), CANCO spectra in *magenta*, NCACO in *orange* and NCACB in *purple* (positive signals) and *green* (negative signals). *Solid lines* represent the assignments used in the sequential walk

All the assigned CA resonances could also be confirmed by a 2D CA(N)COCA spectrum as introduced before (Chevelkov et al. 2013b). A 3D version incorporating a nitrogen chemical shift dimension, i.e. CANCOCA, similar to the experiment presented in (Schuetz et al. 2010) would be useful for applications to larger proteins.

Böckmann, Meier and coworkers described the efficient correlation of well dispersed CA–CB pairs in N(co)CACB and NCACB experiments (Habenstein et al. 2011; Schuetz et al. 2010). We have therefore also performed a BSH-CP version of the N(co)CACB experiment which is a straightforward modification of the NCOCACB experiment as depicted in Fig. 2b (see Table 1 for experimental details and Figure S1 for the pulse scheme). A strip-plot illustrating the corresponding assignment procedure is presented in Fig. 4.

Almost all of the backbone resonances were assigned from Q2 to V70 in the 3D spectra, and the chemical shifts are presented in Supporting Table 1. Similar to previous ssNMR investigations on PEG-precipitated ubiquitin (Seidel et al. 2005; Chevelkov et al. 2013b), peak doubling could be observed for some regions in the MPD-crystallized material studied here as well. The last six C-terminal residues cannot be assigned due to dynamic disorder. In previous studies of MPD-crystallized ubiquitin by ssNMR, only a single set of resonances was reported (Igumenova et al. 2004; Schubert et al. 2006). One of the reasons for this may lie in the slightly different crystallization conditions used. McDermott and coworkers utilized 60 % MPD, 20 mM citrate buffer, at pH 4.0–4.2. In contrast, we used 40 % MPD, 0.2 M $CdCl_2$, at pH 6.5. Furthermore, we note that some of the doubled resonances differ in intensity and can only be observed in spectra with very high S/N.

In conclusion, we have recorded a complete set of high-quality 3D spectra required for unambiguous resonance assignment of the backbone resonances. Due to the

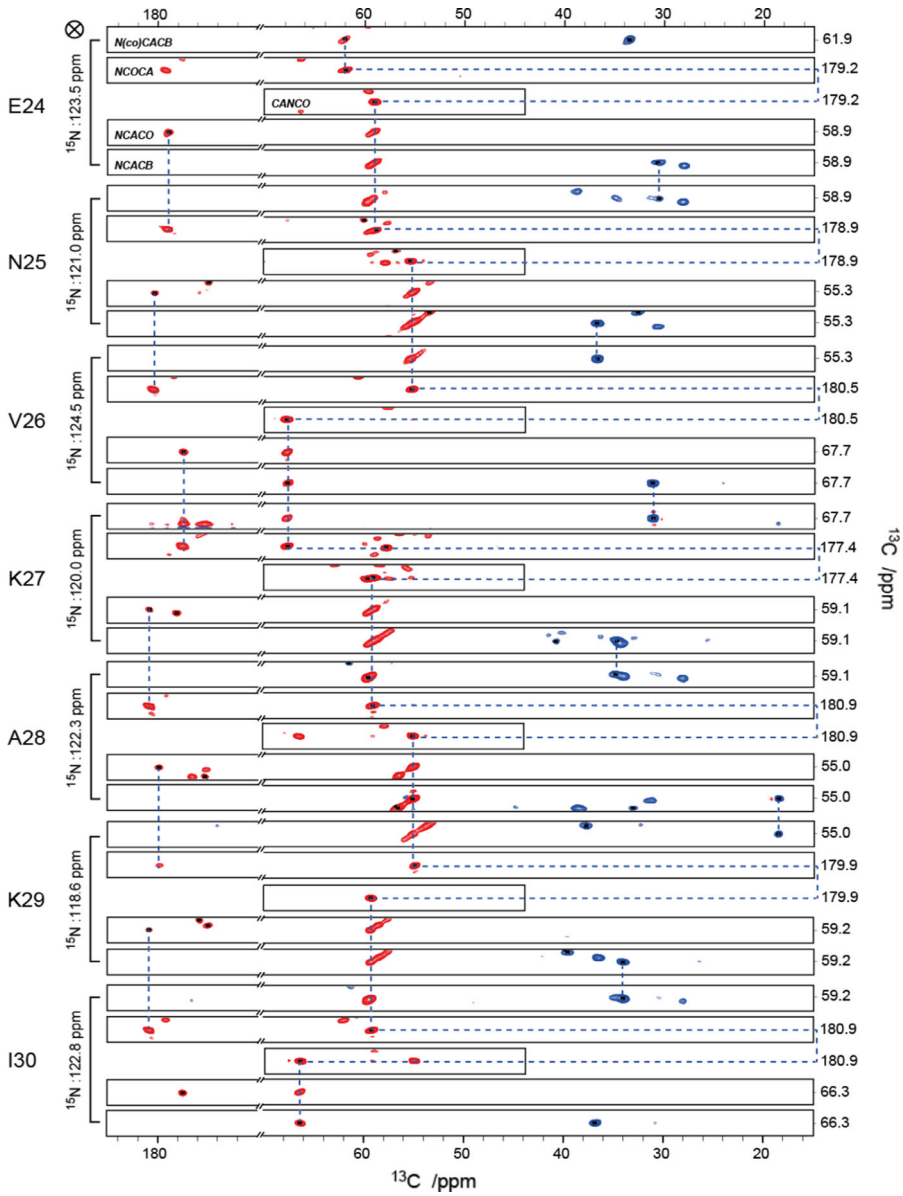

Fig. 4 Strip plot of different 3D experiments showing the sequential walk for the amino acid stretch E24-I30. All the spectra are presented in *red* (positive signals) and *blue* (negative signals)

excellent transfer efficiency provided by BSH-CP, the complete set could be recorded in a short time frame with high sensitivity and resolution.

Materials and methods

Sample preparation

Uniformly [^{13}C,^{15}N]-labeled ubiquitin was expressed and purified as described earlier (Lazar et al. 1997). Around 15 mg of MPD-crystallized material was transferred into a 3.2 mm rotor.

Solid-state NMR experiments

All spectra with the exception of the 3D N(co)CACB spectrum were conducted on a Bruker Avance II 800 MHz standard-bore spectrometer equipped with a commercial (Bruker Biospin) 3.2 mm (^{1}H, ^{13}C, ^{15}N) triple-resonance probe. The N(co)CACB spectrum was measured on a Bruker Avance III 850 MHz wide-bore spectrometer equipped with a commercial (Bruker Biospin) 3.2 mm (^{1}H, X, Y) triple-resonance probe. MAS rates of 20 kHz and 21 kHz were employed for experiments at 800 MHz and 850 MHz, respectively. The probe temperature was set to −25 °C resulting in an effective sample temperature of

about 0 ± 2 °C as measured by the temperature-dependent water proton resonance (Boeckmann et al. 2009). Typical radiofrequency strength of proton, carbon and nitrogen hard pulses was 83.3, 50 and 35.7 kHz, respectively. SPINAL-64 heteronuclear decoupling during isotropic chemical shift evolution was applied on the proton channel with an RF strength of 78 kHz. CW decoupling with an RF strength around 75 kHz was applied during SPECIFIC-CP, BSH-CP and DREAM recoupling. Detailed parameters for all 3D experiments are supplied in Table 1.

Acknowledgments We thank Karin Giller and Brigitta Angerstein for expert technical assistance. This work was supported by the Max Planck Society, the DFG (Emmy Noether Fellowship to A. L.), and the European Union Seventh Framework Program under Grant Agreement 261863 (Bio-NMR). C. S. acknowledges funding from the MPG-CAS Joint Doctoral Promotion Programme. B. H. acknowledges EMBO for a long-term postdoctoral fellowship.

References

Baldus M, Petkova AT, Herzfeld J, Griffin RG (1998) Cross polarization in the tilted frame: assignment and spectral simplification in heteronuclear spin systems. Mol Phys 95(6): 1197–1207. doi:10.1080/002689798166215

Boeckmann A, Gardiennet C, Verel R, Hunkeler A, Loquet A, Pintacuda G, Emsley L, Meier BH, Lesage A (2009) Characterization of different water pools in solid-state NMR protein samples. J Biomol NMR 45(3):319–327. doi:10.1007/s10858-009-9374-3

Chevelkov V, Giller K, Becker S, Lange A (2013a) Efficient CO–CA transfer in highly deuterated proteins by band-selective homonuclear cross-polarization. J Magn Reson 230:205–211. doi:10.1016/j.jmr.2013.02.021

Chevelkov V, Shi C, Fasshuber HK, Becker S, Lange A (2013b) Efficient band-selective homonuclear CO–CA cross-polarization in protonated proteins. J Biomol NMR 56(4):303–311. doi:10.1007/s10858-013-9767-1

Demers J-P, Chevelkov V, Lange A (2011) Progress in correlation spectroscopy at ultra-fast magic-angle spinning: basic building blocks and complex experiments for the study of protein structure and dynamics. Solid State Nucl Magn Reson 40(3):101–113. doi:10.1016/j.ssnmr.2011.07.002

Dusold S, Sebald A (2000) Dipolar recoupling under magic-angle spinning conditions. Annu Rep NMR Spectrosc 41(41):185–264. doi:10.1016/s0066-4103(00)41010-0

Fung BM, Khitrin AK, Ermolaev K (2000) An improved broadband decoupling sequence for liquid crystals and solids. J Magn Reson 142(1):97–101

Goldbourt A (2013) Biomolecular magic-angle spinning solid-state NMR: recent methods and applications. Curr Opin Biotechnol 24(4):705–715. doi:10.1016/j.copbio.2013.02.010

Habenstein B, Wasmer C, Bousset L, Sourigues Y, Schuetz A, Loquet A, Meier BH, Melki R, Boeckmann A (2011) Extensive de novo solid-state NMR assignments of the 33 kDa C-terminal domain of the Ure2 prion. J Biomol NMR 51(3):235–243. doi:10.1007/s10858-011-9530-4

Hodgkinson P, Emsley L (1999) The accuracy of distance measurements in solid-state NMR. J Magn Reson 139(1):46–59. doi:10.1006/jmre 1999.1759

Hong M, Zhang Y, Hu F (2012) Membrane Protein Structure and Dynamics from NMR Spectroscopy. In: Johnson MA, Martinez TJ (eds) Annual review of physical chemistry, vol 63, pp 1–24. doi:10.1146/annurev-physchem-032511-143731

Igumenova TI, McDermott AE, Zilm KW, Martin RW, Paulson EK, Wand AJ (2004) Assignments of carbon NMR resonances for microcrystalline ubiquitin. J Am Chem Soc 126(21):6720–6727. doi:10.1021/ja030547o

Jehle S, Rajagopal P, Bardiaux B, Markovic S, Kuehne R, Stout JR, Higman VA, Klevit RE, van Rossum B-J, Oschkinat H (2010) Solid-state NMR and SAXS studies provide a structural basis for the activation of alpha B-crystallin oligomers. Nat Struct Mol Biol 17(9):1037–1042. doi:10.1038/nsmb.1891

Knight MJ, Pell AJ, Bertini I, Felli IC, Gonnelli L, Pierattelli R, Herrmann T, Emsley L, Pintacuda G (2012) Structure and backbone dynamics of a microcrystalline metalloprotein by solid-state NMR. Proc Natl Acad Sci USA 109(28): 11095–11100. doi:10.1073/pnas.1204515109

Laage S, Marchetti A, Sein J, Pierattelli R, Sass HJ, Grzesiek S, Lesage A, Pintacuda G, Emsley L (2008) Band-Selective ^{1}H–^{13}C Cross-polarization in fast magic angle spinning solid-state NMR spectroscopy. J Am Chem Soc 130(51):17216–17217. doi:10.1021/ja805926d

Lazar GA, Desjarlais JR, Handel TM (1997) De novo design of the hydrophobic core of ubiquitin. Protein Sci 6(6):1167–1178

Loquet A, Sgourakis NG, Gupta R, Giller K, Riedel D, Goosmann C, Griesinger C, Kolbe M, Baker D, Becker S, Lange A (2012) Atomic model of the type III secretion system needle. Nature 486(7402):276–279. doi:10.1038/nature11079

Mainz A, Religa TL, Sprangers R, Linser R, Kay LE, Reif B (2013) NMR spectroscopy of soluble protein complexes at one megadalton and beyond. Angew Chem Int Ed Engl 52(33): 8746–8751. doi:10.1002/anie.201301215

Morcombe CR, Gaponenko V, Byrd RA, Zilm KW (2004) Diluting abundant spins by isotope edited radio frequency field assisted diffusion. J Am Chem Soc 126(23):7196–7197. doi:10.1021/ja047919t

Pauli J, Baldus M, van Rossum B, de Groot H, Oschkinat H (2001) Backbone and side-chain ^{13}C and ^{15}N signal assignments of the alpha-spectrin SH3 domain by magic angle spinning solid-state NMR at 17.6 tesla. ChemBioChem 2(4):272–281. doi:10.1002/1439-7633(20010401)2:4<272:aid-cbic272>3.0.co;2-2

Scholz I, Huber M, Manolikas T, Meier BH, Ernst M (2008) MIRROR recoupling and its application to spin diffusion under fast magic-angle spinning. Chem Phys Lett 460(1–3):278–283. doi:10.1016/j.cplett.2008.05.058

Schubert M, Manolikas T, Rogowski M, Meier BH (2006) Solid-state NMR spectroscopy of 10 % C-13 labeled ubiquitin: spectral simplification and stereospecific assignment of isopropyl groups. J Biomol NMR 35(3):167–173. doi:10.1007/s10858-006-9025-x

Schuetz A, Wasmer C, Habenstein B, Verel R, Greenwald J, Riek R, Boeckmann A, Meier BH (2010) Protocols for the sequential solid-state NMR spectroscopic assignment of a uniformly labeled 25 kDa protein: HET-s(1-227). ChemBioChem 11(11): 1543–1551. doi:10.1002/cbic.201000124

Seidel K, Etzkorn M, Heise H, Becker S, Baldus M (2005) High-resolution solid-state NMR studies on uniformly ^{13}C, ^{15}N-labeled ubiquitin. ChemBioChem 6(9):1638–1647. doi:10.1002/cbic.200500085

Sengupta I, Nadaud PS, Helmus JJ, Schwieters CD, Jaroniec CP (2012) Protein fold determined by paramagnetic magic-angle spinning solid-state NMR spectroscopy. Nat Chem 4(5):410–417. doi:10.1038/nchem.1299

Shaka AJ, Keeler J, Frenkiel T, Freeman R (1983) An improved sequence for broad-band decoupling—WALTZ-16. J Magn Reson 52(2):335–338

Shi L, Ahmed MAM, Zhang W, Whited G, Brown LS, Ladizhansky V (2009) Three-dimensional solid-state NMR study of a seven-helical integral membrane proton pump-structural insights. J Mol Biol 386(4):1078–1093. doi:10.1016/j.jmb.2009.01.011

Sperling LJ, Berthold DA, Sasser TL, Jeisy-Scott V, Rienstra CM (2010) Assignment strategies for large proteins by magic-angle spinning NMR: the 21-kDa disulfide-bond-forming enzyme DsbA. J Mol Biol 399(2):268–282. doi:10.1016/j.jmb.2010.04.012

Takegoshi K, Nakamura S, Terao T (2001) C-13-H-1 dipolar-assisted rotational resonance in magic-angle spinning NMR. Chem Phys Lett 344(5–6):631–637. doi:10.1016/s0009-2614(01)00791-6

Tycko R (2011) Solid-state NMR studies of amyloid fibril structure. In: Leone SR, Cremer PS, Groves JT, Johnson MA (eds) Annual review of physical chemistry, vol 62, pp 279–299. doi:10.1146/annurev-physchem-032210-103539

Ullrich SJ, Hellmich UA, Ullrich S, Glaubitz C (2011) Interfacial enzyme kinetics of a membrane bound kinase analyzed by real-time MAS-NMR. Nat Chem Biol 7(5):263–270. doi:10.1038/nchembio.543

Verel R, Ernst M, Meier BH (2001) Adiabatic dipolar recoupling in solid-state NMR: the DREAM scheme. J Magn Reson 150(1):81–99. doi:10.1006/jmre 2001.2310

Vijayan V, Demers J-P, Biernat J, Mandelkow E, Becker S, Lange A (2009) Low-power solid-state NMR experiments for resonance assignment under fast magic-angle spinning. ChemPhysChem 10(13):2205–2208. doi:10.1002/cphc.200900439

Wasmer C, Lange A, Van Melckebeke H, Siemer AB, Riek R, Meier BH (2008) Amyloid fibrils of the HET-s(218–289) prion form a beta solenoid with a triangular hydrophobic core. Science 319(5869):1523–1526. doi:10.1126/science.1151839